density must be very small, some hundredfold less than that of our atmosphere at the surface of the earth; but with this restriction there seems to be no bar to the existence of a lunar atmosphere of considerable extent, and it is difficult to explain certain observations without assuming the existence of some atmosphere."

2. T. Morgan and A. Stern, *Eos* **72**, 225 (1991). In comparison to the Earth's total atmospheric density of ~$10^{19}$ molecules per cubic centimeter at the surface, the lunar value is lower by a factor of $10^{-12}$.
3. A. E. Potter and T. H. Morgan, *Science* **241**, 675 (1988).
4. A. Tyler, R. Kozlowski, D. Hunten, *Geophys. Res. Lett.* **15**, 1141 (1988).
5. The mean lunar radius ($R_m$) is 1738 km; Na was detected at ~1200 km by A. Potter and T. Morgan (*ibid.*, p. 1515).
6. D. Hunten, R. Kozlowski, A. Sprague, *ibid.* **18**, 2101 (1991).
7. A. Sprague, R. Kozlowski, D. Hunten, W. Wells, R. Grosse, *Icarus* **96**, 27 (1992).
8. A. Potter and T. Morgan, *Geophys. Res. Lett.* **18**, 2089 (1991).
9. T. Morgan and D. Shemansky, *J. Geophys. Res.* **96**, 1351 (1991).
10. M. Mendillo, J. Baumgardner, B. Flynn, *Nature* **348**, 312 (1990).
11. B. Flynn, M. Mendillo, J. Baumgardner, *Icarus* **99**, 115 (1992).
12. M. Mendillo, B. Flynn, J. Baumgardner, *Adv. Space Res.*, in press.
13. M. Mendillo, J. Baumgardner, B. Flynn, *Geophys. Res. Lett.* **18**, 2097 (1991).
14. W.-H. Ip, *ibid.*, p. 2093.
15. Detailed analysis and modeling of these and other image sets are under way: B. Flynn, unpublished results; W. Smyth, personal communication.
16. If the emergent Na velocity distribution is Maxwellian, the root mean square velocity $V_{rms} = (3kT/m)^{1/2}$ (*m* is mass) reduces to *V* (in kilometers per second) = $0.033\sqrt{T}$ (in kelvin).
17. This work was supported, in part, by a grant from the National Aeronautics and Space Administration Space Physics Division and by funds provided for the Center for Space Physics at Boston University. We are grateful for the assistance of J. Baumgardner, for discussion with A. Sprague and D. Hunten, and for the insightful comments of a referee. Both authors are Guest Observers at the McDonald Observatory, and we acknowledge the continued cooperation of observatory personnel in making these observations possible.

15 March 1993; accepted 20 May 1993

---

# Relation Between Bond-Length Alternation and Second Electronic Hyperpolarizability of Conjugated Organic Molecules

Seth R. Marder,* Joseph W. Perry,* Grant Bourhill, Christopher B. Gorman, Bruce G. Tiemann, Kamjou Mansour

**The solvent dependence of the second hyperpolarizability, γ, of a variety of unsaturated organic compounds has been measured by third harmonic generation at 1907 nanometers. It is seen that the measured γ is a function of solvent polarity. These solvent-dependent hyperpolarizabilities are associated with changes in molecular geometry from a highly bond-length alternated, polyene-like structure for a formyl-substituted compound in nonpolar solvents, to a cyanine-like structure, with little bond-length alternation, for a dicyanovinyl-substituted compound in polar solvents. By tuning bond-length alternation, γ can be optimized in either a positive or negative sense for polymethine dyes of a given conjugation length.**

The development of materials with third-order optical nonlinearities has been the focus of much recent research (*1, 2*). Such materials are of interest for a variety of optical switching and processing applications. However, materials with sufficiently high nonlinearities for most of these applications have not yet been identified (*3*). In contrast to the relatively well-defined structure-property relationships (*1, 2, 4*) used to guide the design of molecules for second-order nonlinear optical applications, such relationships for third-order nonlinear optical chromophores are lacking (*5*). Theoretical and experimental studies (*4*) suggest that bond-length alternation, <Δr> (defined as the difference between the average lengths of carbon-carbon single and double bonds in a polymethine chain) is a useful structural parameter to vary in attempts to optimize the first hyperpolarizability, β, for organic molecules. Recent semiempirical molecular orbital calculations support this hypothesis and predict that trends for the second hyperpolarizability, γ, are associated with bond-length alternation (*6*). For example, electric field–dependent calculations of geometry and second hyperpolarizability indicate that for highly bond-length alternated molecules, such as polyenes, γ is positive; as a function of increasing polarization and decreasing <Δr>, γ first increases, peaks in a positive sense, decreases, crosses through zero and ultimately peaks in a negative sense at the cyanine-limit of zero bond-length alternation (Fig. 1). To develop structure-property relationships for γ and to test these predictions, we examined a series of molecules whose bond-length alternation spans the range accessible to organic molecules containing polymethine chains.

We report γ values for a set of molecules (**1** to **4** and **6**, Fig. 2) ranging from polyenes, for which the bond-length alternation equals 0.11 Å (as determined crystallographically, from diphenyl octatetraene (*7*) and octatetraene (*8*) to cyanines, for which <Δr> is essentially zero, again determined crystallographically (*9, 10*). In order to tune the bond-length alternation from the polyene limit to the cyanine limit, we used two donor-acceptor polyenes with acceptors of differing strength in solvents ranging from nonpolar to highly polar. Such solvent-dependent changes in structure can be understood in terms of simple resonance structure arguments (*11*). The ground state of a polymethine dye can be described in terms of contributions of two limiting charge transfer resonance structures (Fig. 2). The equilibrium structure of the ground state represents a weighted average of the limiting resonance structures and approaches a bond-equivalent structure for an equal mixture, as is the case for cyanines. For donor-acceptor compounds such as **3** and **4**, polar solvents can stabilize charge separation and would increase the contribution of the charge-separated form to the ground state. Thus, donor-acceptor molecules with strong acceptors, in solvents of high polarity, would be expected to exhibit diminished bond-length alternation relative to molecules with weaker acceptors in low polarity solvents.

$^1$H nuclear magnetic resonance (NMR) (*12*), Raman (*13*), and electronic absorption (*14*) spectroscopic studies, in conjunc-

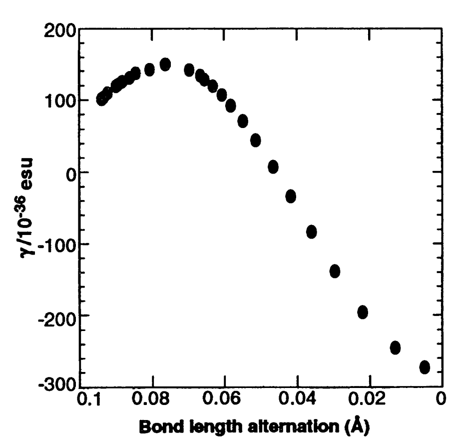

**Fig. 1.** Plot of γ versus <Δr>, generated with an AM1 geometry optimization (in the MOPAC package) for **3** in the presence of a static electric field of varying strength (*6*). For each value of the static field, and thus <Δr>, γ was calculated with a finite-field procedure; esu, electrostatic unit.

---

S. R. Marder, C. B. Gorman, B. G. Tiemann, Jet Propulsion Laboratory, California Institute of Technology, Pasadena, CA 91109 and The Beckman Institute, California Institute of Technology, Pasadena, CA 91125.

J. W. Perry, G. Bourhill, K. Mansour, Jet Propulsion Laboratory, California Institute of Technology, Pasadena, CA 91109.

*To whom correspondence should be addressed.

tion with x-ray crystallography (*13*), have shown that the bond-length alternation in polymethine compounds can be tuned by solvent. For **3** and **4**, $^1$H NMR spectroscopy of the solvent dependence of the three bond proton-proton coupling constants ($^3J_{HH}$) along the polymethine chains provides evidence for the transition from a polyene-like geometry to a cyanine-like geometry. For a polyene ($<\Delta r> \cong 0.11$ Å) the difference between CH=CH and CH–CH coupling constants, $\Delta[^3J_{HH}]$, is approximately 4 to 5 Hz. For a cyanine ($<\Delta r> \cong 0$ Å), the difference in coupling constants becomes negligible. For **3** (in nonpolar solvents) $\Delta[^3J_{HH}] \cong 3.6$ Hz, and drops to approximately 2.5 Hz in a polar solvent such as $CH_3OH$. For **4** in $CCl_4$ $\Delta[^3J_{HH}] \cong 1.0$ Hz, and in $CH_3OH$, $\Delta[^3J_{HH}] \leq 0.2$ Hz.

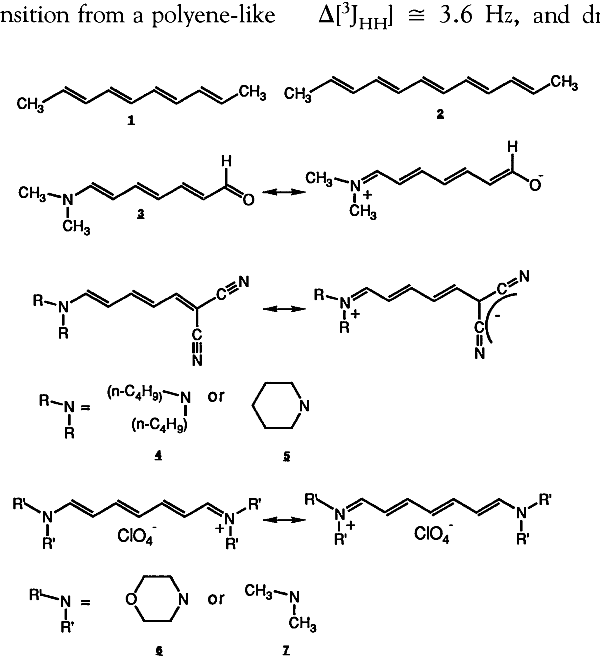

**Fig. 2.** Structures of the compounds investigated in this study. For the polymethine dyes, with an odd number of π-conjugated atoms, two canonical resonance structures are given.

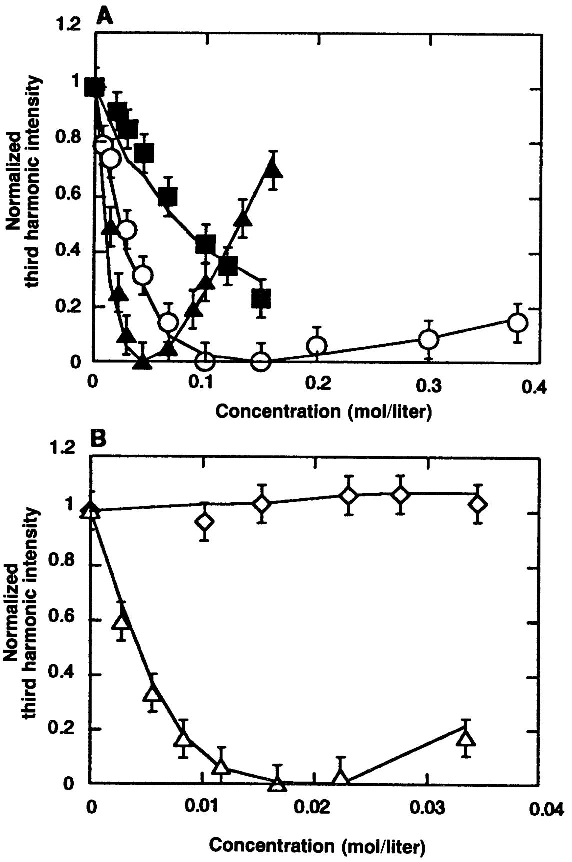

**Fig. 3.** Experimental (symbols) and theoretical best fit (solid line) normalized third harmonic intensities as a function of concentration for (**A**) **4** in $CCl_4$ (squares), in $CH_2Cl_2$ (circles), in $CH_3CN$ (triangles), and for (**B**) **2** in $C_6H_6$ (diamonds) and **6** in $CH_3CN$ (triangles). The magnitude and phase of γ was determined with a model developed by Kajzar (*18*). Best fits were obtained with the use of the real and imaginary parts of the solute hyperpolarizability as fitting parameters. Experimentally determined coherence lengths were used as fixed parameters. All other parameters were known or determined separately and fixed. For all the solutions studied, the theoretical normalized third harmonic intensities closely matched the experimentally observed intensities using only a real, nonzero solute hyperpolarizability.

The carbon-carbon bond lengths for compounds **3** and **5** (a derivative closely related to **4**) have been determined in the solid state by x-ray diffraction methods (*13*). For **3**, the bond-length alternation is substantially reduced ($<\Delta r> = 0.06$ Å) relative to simple polyenes ($<\Delta r> = 0.11$ Å). For the dicyanovinyl-substituted compound, **5**, $<\Delta r>$ drops to 0.01 Å, indicating that the solid-state structure no longer resembles a bond alternate polyene but instead resembles a bond-equivalent cyanine.

We obtained the Raman spectra of compounds **1** to **5** and the cyanine **7** in the solid state and in solvents of varying polarity (*13*). The polyene spectrum showed two strong bands (*15*) at about 1600 cm$^{-1}$ (C=C stretch) and 1150 cm$^{-1}$ (C–C stretch and C–H in-plane bend). The spectrum of the cyanine **7** is different, with several strong bands of intermediate frequency, the strongest of which occurs at approximately 1400 cm$^{-1}$. The spectrum of **3** in a polar solvent showed a reduced frequency for the C=C stretch and slightly enhanced intensity for the intermediate bands relative to the simple polyene spectrum, and was qualitatively similar to its solid-state spectrum, suggesting that $<\Delta r>$ for **3** in polar solvents approaches the solid-state value (0.06 Å). In contrast, the spectrum of **5** in a nonpolar solvent was qualitatively similar to that of **3** in both the solid state and in polar solvents. However, the bands in the region around 1400 cm$^{-1}$ were more intense than those for **3** in the solid state; this difference suggests that $<\Delta r>$ for **5** in nonpolar solvents is $\leq 0.06$ Å. On the other hand, the spectrum of **5** in polar solvents, showed enhanced intensity of the intermediate bands and appeared qualitatively similar to both its solid-state spectrum, where $<\Delta r>$ is 0.01 Å, and the cyanine spectrum.

Additionally, the electronic absorption spectra of **4** were consistent with an evolution of its ground state toward a cyanine-like structure as the solvent polarity is increased. The Franck-Condon distribution of **4** in $CH_3OH$ was similar to that of the cyanine **6** and indicated that the change in equilibrium vibrational coordinate on electronic excitation is small. In $CCl_4$, the vibronic structure observed for **4** is intermediate between that observed for the polyene **1** and the cyanine **6**.

The NMR, Raman, electronic absorption, and crystallographic data provided strong evidence that solvent polarity can be used to tune the geometry of donor-acceptor polyenes from a polyene-like to a cyanine-like structure. In particular, bond-length alternation decreases in the following order: for **1**, **2**, and **3** (in nonpolar solvents), $<\Delta r> \cong 0.11$ Å and is greater than that for **3** (in the solid state) or **3** (in polar solvents), where $<\Delta r> \cong 0.06$ Å. For **4** and **5** (in nonpolar solvents), $<\Delta r> \leq 0.06$ Å and is greater than that for **4** and **5** (in polar solvents) and for **5** (in the solid state) where $<\Delta r> \cong 0.01$ Å. Finally, for **6** or **7** $<\Delta r> \cong 0$ Å.

We measured the second hyperpolarizability, $\gamma$, of **1** to **4** and **6**, in solvents of varying polarity, by third harmonic generation (THG) using a fundamental wavelength of 1907 nm. We performed the THG measurements with an apparatus described earlier (*16, 17*). Concentration-dependent measurements were employed for the determination of the magnitude and phase of $\gamma$ (Fig. 3). The results (Table 1) show that $\gamma$ for the linear polyenes, **1** and **2**, is positive whereas it is negative for the cyanine, **6**, in the same solvent consistent with earlier measurements (*19*). The $\gamma$ values for **1**, **2**, and **6** are relatively insensitive to changes in the solvent polarity. In Fig. 4, $\gamma$ values for **3** and **4** are plotted as a function of a linear solvent polarity parameter [Reichardt's normalized $E_T(30)$ scale (*20*)]. The plots have been included to give an indication of the shape the dependence of $\gamma$ on bond-length alternation.

The trends observed for **3** and **4** as a function of solvent polarity (and hence bond-length alternation) qualitatively agree with those from finite field calculations (Fig. 1). Understanding of the origin of the observed and calculated trends in $\gamma$ can be obtained from a simple three-state model for $\gamma$ (*21–23*), derived from static perturbation theory, in which

$$\gamma \propto \underset{\text{N1}}{-\left(\frac{\mu_{ge}^4}{E_{ge}^3}\right)} + \underset{\text{P1}}{\left(\frac{\mu_{ge}^2\,\mu_{ee'}^2}{E_{ge}^2\,E_{ge'}}\right)} + \underset{\text{P2}}{\left(\frac{\mu_{ge}^2(\mu_{ee}-\mu_{gg})^2}{E_{ge}^3}\right)} \qquad (1)$$

where g labels the ground state, e and e′ label the two excited states, and $\mu$ and E are the dipole matrix element and transition energy, respectively, between the labeled states. Hence, the three-state expression for $\gamma$ is comprised of three terms, one negative (N1) and two positive (P1 and P2) in sign. The P2 term is zero for centrosymmetric polyenes where $\mu_{ee} = \mu_{gg} = 0$ and negligible in the cyanine-limit (*4*). When the first term (N1) is dominant, the molecule will exhibit a negative $\gamma$, as is the case for the cyanine **6**. For polyenes (**1** and **2**) $|P1| > |N1|$ and $\gamma$ is positive. For donor-acceptor polyenes (such as **3** and **4**), P2 will in general be non-zero and all three terms in Eq. 1 must be considered. P2 can be related to the two-state expression for $\beta$ {where $\beta \propto [\mu_{ge}^2(\mu_{ee} - \mu_{gg})/E_{ge}^2]$} by $P2 = \beta(\mu_{ee} - \mu_{gg})/E_{ge}$. $\beta$ can be calculated for a four orbital model as a function of the mixing of neutral and charge transfer states and was shown to exhibit a peaked behavior as a function of the mixing, due largely to a peak in $(\mu_{ee} - \mu_{gg})$ (*4*). The P2 term is thus expected to increase from zero, reach a maximum, and decrease to zero as the bond-length alternation of the donor-acceptor polyene is reduced from polyene-like to cyanine-like. Therefore, increased solvent polarity leads to an increase in $\gamma$ as the P2 contribution increases, from the polyene bond alternation limit, and $|P1|$ is still greater than $|N1|$ (*23, 24*). With further increase in solvent polarity (and decrease in bond-length alternation), $\gamma$ will reach a peak and begin to decrease as P2 peaks and P1 + N1 decreases. Such behavior was observed for **3**. As bond-length alternation continues to decrease, $\gamma$ will go through zero when N1 = P1 + P2 and to negative values when N1 dominates P1 + P2, because P2 approaches zero and $|N1| > P1$ near the cyanine limit. This model explains the behavior for **4**, which has a stronger acceptor moiety than **3** and therefore intrinsically less bond-length alternation. Thus, these experimental results qualitatively confirm theoretical predictions made by three-state models (*21–23*) and by electric field–dependent hyperpolarizability calculations (**6**). Finally, this study provides specific structural guidelines for the optimization of $\gamma$, in a positive or negative sense, for polymethine dyes of a given length.

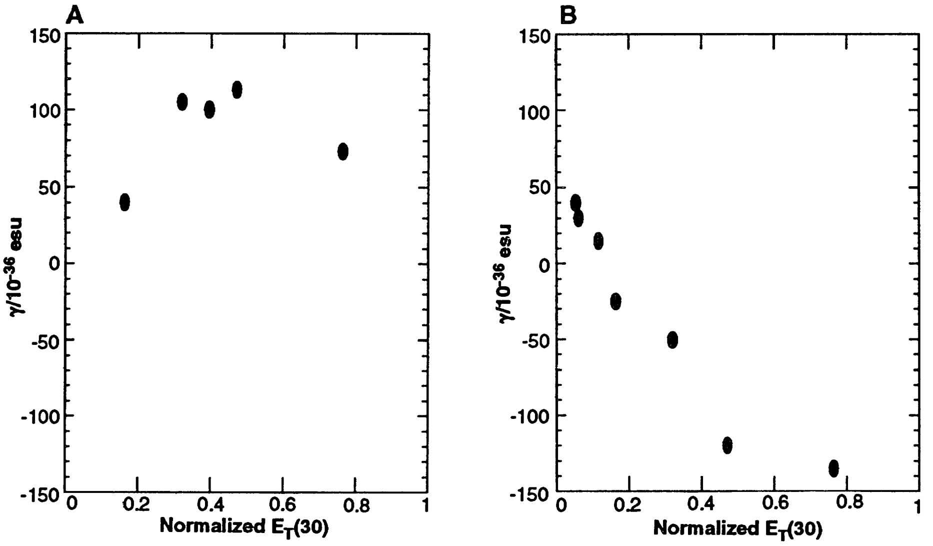

**Fig. 4.** Plot of $\gamma$ versus Reichardt's normalized $E_T$ (30) scale for (**A**) **3** and (**B**) **4**.

**Table 1.** Solvent-dependent second hyperpolarizabilities (units of $10^{-36}$ esu) for compounds **1** to **4** and **6**, with an estimated error of ±15%. Compounds were determined to be >95% pure by $^1H$ NMR spectroscopy. Solvent polarity increases (bond-length alternation decreases) from right to left. Solubility limitations prevented the determination of $\gamma$ for some molecules in certain solvents.

| Compound | Solvent | | | | | | | |
|---|---|---|---|---|---|---|---|---|
| | $CH_3OH$ | $CH_3CN$ | $CH_3CN$-$CH_2Cl_2$* | $CH_2Cl_2$ | Dioxane | $C_6H_6$ | $C_6H_6$-*n*-$C_6H_{14}$* | $CCl_4$ |
| **1** | — | — | — | +27 | +25 | +34 | — | — |
| **2** | — | — | — | +72 | +70 | +60 | — | — |
| **3** | +73 | +113 | +100 | +105 | +40 | — | — | — |
| **4** | −135 | −120 | — | −50 | −25 | +15 | +30 | +40 |
| **6** | — | −370 | — | −325 | — | — | — | — |

*For both the $CH_3CN$-$CH_2Cl_2$ and the $C_6H_6$-*n*-$C_6H_{14}$ mixtures, the compositions were 1:1 by mole fraction.

## REFERENCES AND NOTES

1. S. R. Marder, J. E. Sohn, G. D. Stucky, Eds., *Materials for Nonlinear Optics: Chemical Perspectives, ACS Symposium Series 455* (American Chemical Society, Washington, DC, 1991).
2. P. N. Prasad and D. J. Williams, Eds., *Introduction to Nonlinear Optical Effects in Molecules and Polymers* (Wiley, New York, 1991).
3. G. T. Boyd, *J. Opt. Soc. Am. B.* **6**, 685 (1989).
4. S. R. Marder, D. N. Beratan, L.-T. Cheng, *Science* **252**, 103 (1991).
5. The role of degenerate ground states has been used to explain the large third-order susceptibility of polyacetylene. However this elegant model does not provide specific structural guidelines as to how to optimize $\gamma$ in either a positive or negative sense for molecules of a finite length. T. W. Hagler and A. J. Heeger, *Chem. Phys. Lett.* **189**, 333 (1991); C Halvorson, T. W. Hagler, D. Moses, Y. Cao, A. J. Heeger, *Chem. Phys. Lett.* **200**, 364 (1992).

6. S. R. Marder, C. B. Gorman, B. G. Tiemann, L.-T. Cheng, *Proc. SPIE* **1775**, 19 (1993); C. B. Gorman and S. R. Marder, in preparation.
7. W. Drenth and E. H. Wiebenga, *Acta Crystallogr.* **8**, 755 (1955).
8. R. H. Baughman, B. E. Kohler, I. J. Levy, C. W. Spangler, *Synth. Methods* **11**, 37 (1985).
9. P. Groth, *Acta Chem. Scand. B* **41**, 547 (1987).
10. F. Chentli-Bechikha, J. P. Declercq, G. Germain, M. V. Meersscha, *Cryst. Struct. Comm.* **6**, 421 (1977).
11. L. G. S. Brooker *et al.*, *J. Am. Chem. Soc.* **73**, 5332 (1951).
12. R. Radeglia and S. Dahne, *J. Mol. Struct.* **5**, 399 (1970).
13. S. R. Marder *et al. J. Am. Chem. Soc.* **115**, 2525 (1993).
14. S. Schneider, *Ber. Buns. Ges.* **80**, 218 (1976).
15. H. E. Schaffer, R. R. Chance, R. J. Silbey, K. Knoll, R. R. Schrock, *J. Chem. Phys.* **94**, 4161 (1991)
16. F. Kajzar and J. Messier, *Rev. Sci. Instrum.* **58**, 2081 (1987).
17. S. R. Marder, J. W. Perry, F. L. Klavetter, R. H. Grubbs, in *Organic Materials for Nonlinear Optics*, R. A. Hann and D. Bloor, Eds. (Royal Society of Chemistry, London, 1989), pp. 288–294.
18. F. Kajzar, in *Nonlinear Optics of Organics and Semiconductors*, T. Kobayashi, Ed. (Springer-Verlag, Berlin, 1989), pp. 108–119.
19. S. H. Stevenson, D. S. Donald, G. R. Meredith, in *Nonlinear Optical Properties of Polymers, Mat. Res. Soc. Symp. Proc. 109* (Materials Research Society, Pittsburgh, 1988), pp. 103–108.
20. Y. Marcus, *J. Soln. Chem.* **20**, 929 (1991).
21. B. M. Pierce, *Proc. SPIE* **1560**, 148 (1991).
22. C. W. Dirk, L.-T. Cheng, M. G. Kuzyk, *Int. J Quant. Chem.* **43**, 27 (1992).
23. Enhancement of γ by the P2 term has been discussed previously: A. F. Garito, J. R. Heflin, K. Y Yong, O. Zamani-khamiri, *Proc SPIE* **971**, 2 (1988).
24. Increased γ in donor-acceptor–conjugated organics relative to centrosymmetric analogs has been observed experimentally: C. W. Spangler, K. O. Havelka, M. W. Becker, T. A. Kelleher, L.-T. Cheng, *Proc. SPIE* **1560**, 139 (1991); L.-T. Cheng *et al.*, *J. Phys. Chem.* **95**, 10631 (1991); L.-T. Cheng *et al.*, *ibid.*, p. 10643.

25. The research was performed, in part, at the Center for Space Microelectronics Technology, Jet Propulsion Laboratory (JPL), California Institute of Technology, and was supported, in part, by the Strategic Defense Initiative Organization–Innovative Science and Technology Office, through an agreement with the National Aeronautics and Space Administration (NASA). Support at the Beckman Institute by the Air Force Office of Scientific Research (grant F49620-92-J-0177) is also acknowledged. C.B.G. thanks the JPL director's office for a postdoctoral fellowship. G.B. thanks the National Research Council and NASA for a resident research associateship at JPL.

29 January 1993; accepted 19 May 1993

---

# Complex Patterns in a Simple System

John E. Pearson

**Numerical simulations of a simple reaction-diffusion model reveal a surprising variety of irregular spatiotemporal patterns. These patterns arise in response to finite-amplitude perturbations. Some of them resemble the steady irregular patterns recently observed in thin gel reactor experiments. Others consist of spots that grow until they reach a critical size, at which time they divide in two. If in some region the spots become overcrowded, all of the spots in that region decay into the uniform background.**

Patterns occur in nature at scales ranging from the developing *Drosophila* embryo to the large-scale structure of the universe. At the familiar mundane scales we see snowflakes, cloud streets, and sand ripples. We see convective roll patterns in hydrodynamic experiments. We see regular and almost regular patterns in the concentrations of chemically reacting and diffusing systems (*1*). As a consequence of the enormous range of scales over which pattern formation occurs, new pattern formation phenomenon is potentially of great scientific interest. In this report, I describe patterns recently observed in numerical experiments on a simple reaction-diffusion model. These patterns are unlike any that have been previously observed in theoretical or numerical studies.

The system is a variant of the autocatalytic Selkov model of glycolysis (*2*) and is due to Gray and Scott (*3*). A variety of spatio-temporal patterns form in response to finite-amplitude perturbations. The response of this model to such perturbations was previously studied in one space dimension by Vastano *et al.* (*4*), who showed that steady spatial patterns could form even when the diffusion coefficients were equal. The response of the system in one space dimension is nontrivial and depends both on the control parameters and on the initial perturbation. It will be shown that the patterns that occur in two dimensions range from the well-known regular hexagons to irregular steady patterns similar to those recently observed by Lee *et al.* (*5*) to chaotic spatio-temporal patterns. For the ratio of diffusion coefficients used, there are no stable Turing patterns.

Most work in this field has focused on pattern formation from a spatially uniform state that is near the transition from linear stability to linear instability. With this restriction, standard bifurcation-theoretic tools such as amplitude equations have been developed and used with considerable success (*6*). It is unclear whether the patterns presented in this report will yield to these now-standard technologies.

The Gray-Scott model corresponds to the following two reactions:

$$\begin{aligned} \mathrm{U} + 2\mathrm{V} &\rightarrow 3\mathrm{V} \\ \mathrm{V} &\rightarrow \mathrm{P} \end{aligned} \tag{1}$$

Both reactions are irreversible, so P is an inert product. A nonequilibrium constraint is represented by a feed term for U. Both U and V are removed by the feed process. The resulting reaction-diffusion equations in dimensionless units are:

$$\begin{aligned} \frac{\partial U}{\partial t} &= D_u \nabla^2 U - UV^2 + F(1 - U) \\ \frac{\partial V}{\partial t} &= D_v \nabla^2 V + UV^2 - (F + k)V \end{aligned} \tag{2}$$

where $k$ is the dimensionless rate constant of the second reaction and $F$ is the dimensionless feed rate. The system size is 2.5 by 2.5, and the diffusion coefficients are $D_u = 2 \times 10^{-5}$ and $D_v = 10^{-5}$. The boundary conditions are periodic. Before the numerical results are presented, consider the behavior of the reaction kinetics which are described by the ordinary differential equations that result upon dropping the diffusion terms in Eq. 2.

In the phase diagram shown in Fig. 1, a trivial steady-state solution $U = 1, V = 0$ exists and is linearly stable for all positive $F$ and $k$. In the region bounded above by the solid line and below by the dotted line, the system has two stable steady states. For fixed $k$, the nontrivial stable uniform solution loses stability through saddle-node bifurcation as $F$ is increased through the upper solid line or by Hopf bifurcation to a periodic orbit as $F$ is decreased through the dotted line. [For a discussion of bifurcation theory, see chapter 3 of (*7*).] In the case at hand, the bifurcating periodic solution is stable for $k < 0.035$ and unstable for $k > 0.035$. There are no periodic orbits for parameter values outside the region enclosed by the solid line. Outside this region the system is excitable. The trivial state is linearly stable and globally attracting. Small perturbations decay exponentially but larger perturbations result in a long excursion through phase space before the system returns to the trivial state.

The simulations are forward Euler integrations of the finite-difference equations resulting from discretization of the diffusion operator. The spatial mesh consists of 256 by 256 grid points. The time step used is 1. Spot checks made with meshes as large as 1024 by 1024 and time steps as small as 0.01 produced no qualitative difference in the results.

Initially, the entire system was placed in the trivial state ($U = 1, V = 0$). The 20 by 20 mesh point area located symmetrically

---

Center for Nonlinear Studies, Los Alamos National Laboratory, Los Alamos, NM 87545.